Inorganic Chemistry

Article

pubs.acs.org/IC

Mixed Valency in Quadruple Hydrogen-Bonded Dimers of Bis(biimidazolate)dirhodium Complexes

Jin-Long, Yuki Matsuda, Kazuhiro Uemura, and Masahiro Ebihara*

Department of Chemistry and Biomolecular Science, Faculty of Engineering, Gifu University, Yanagido, Gifu 501-1193, Japan

Supporting Information

ABSTRACT: Dirhodium complexes with biimidazole (H_2bim) ligands $[Rh_2(O_2CR)_2(H_2bim)_2Cl_2]$ (R = Bu ($[\mathbf{1}Cl_2]$), Pr ($[\mathbf{2}Cl_2]$)), $[Rh_2(O_2CBu)_2(H_2bim)_2](PF_6)_2$ ($[\mathbf{1}](PF_6)_2$), $[Rh_2(O_2CBu)_2(H_2bim)_2(PPh_3)_2](PF_6)_2$ ($[\mathbf{1}(PPh_3)_2](PF_6)_2$), and $[Rh_2(O_2CPr)_2(H_2bim)_2(PPh_3)_2]Cl_2$ ($[\mathbf{2}(PPh_3)_2]Cl_2$) have been synthesized. Deprotonation of the biimidazole complexes afforded the quadruply hydrogen-bonded dimers of the biimidazolate complexes $[Rh_2(O_2CR)_2(Hbim)_2(PPh_3)_2]_2$ (R = Bu ($[\mathbf{1}'(PPh_3)_2]_2$) and Pr ($[\mathbf{2}'(PPh_3)_2]_2$)). Complementary hydrogen bonds between the $Hbim^-$ ligands are not coplanar because the $Hbim^-$ ions in one dirhodium complex are not parallel (the dihedral angle between them is ca. 15°). A cyclic voltammogram of $[\mathbf{1}'(PPh_3)_2]_2$ shows two sets of two consecutive oxidation waves in CH_2Cl_2. The one-electron-oxidized species of $[\mathbf{1}'(PPh_3)_2]_2$ showed no intervalence charge-transfer band in the electronic spectrum and an axially symmetrical ESR spectrum with hyperfine structure because of two phosphorus atoms. These observations show that the odd electron is localized in a σ(Rh−Rh) orbital on one dirhodium unit. Theoretical calculations indicate that an oxidized complex $[Rh_2(O_2CMe)_2(bim)_2(PMe_3)_2]^-$ hydrogen bonded with a biimidazole complex $[Rh_2(O_2CMe)_2(H_2bim)_2(PMe_3)_2]^{2+}$ was a stable mixed-valence complex.

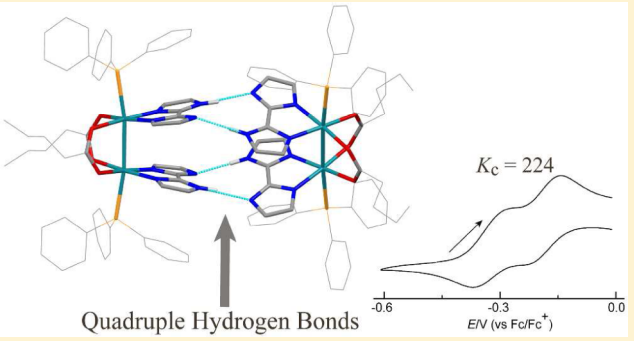

INTRODUCTION

Mixed-valence complexes have received much attention in coordination chemistry over the last four decades. Recently, a few examples of mixed valency in hydrogen-bonded dimer complexes have been reported. Kaifer and co-workers reported a hydrogen-bonded dimer of ferrocene complexes. The one-electron-oxidized dimer species showed an intervalence charge-transfer (IVCT) band at 1200 nm, indicating that there is electronic communication between the ferrocene centers.[1] Kubiak and co-workers also reported electronically communicated mixed valency in the hydrogen-bonded dimer of triruthenium complexes.[2,3] In 2007 Tadokoro and co-workers reported a hydrogen-bonded dimerized complex $[Re^{III}Cl_2(PBu_3)_2(Hbim)]_2$ (H_2bim = biimidazole) that showed two successive one-electron oxidation and two successive one-electron reduction processes, whereas the monomer showed one-electron oxidation and reduction processes.[4] They explained that the first oxidation step generated the asymmetrically protonated mixed-valence species $[Re^{IV}Cl_2(PBu_3)_2(bim)][Re^{III}Cl_2(PBu_3)_2(H_2bim)]^+$, and the first reduction process formed $[Re^{III}Cl_2(PBu_3)_2(bim)]$-$[Re^{II}Cl_2(PBu_3)_2(H_2bim)]^-$. Synchronized motion of proton and electron stabilized this type of mixed-valence compound. Patmore and co-workers also showed the stability of the proton-coupled mixed-valence states for the hydrogen-bonded dimers of dimetal complexes $[M_2(TiPB)_3(HDON)]_2$ (M = Mo, W; TiPB = 2,4,6-triisopropylbenzoate; H_2DON = 2,7-dihydroxy-1,8-naphthyridine) and related compounds.[5,6] All of the reported mixed-valence dimer complexes are doubly or quadruply hydrogen-bonded dimers in which the self-complementary hydrogen bonds lie in the same plane.

We investigated the electronic structures of paddlewheel dirhodium complexes and syntheses of assembled complexes using these complexes as modules.[7] The dirhodium complexes are useful modules because they change the highest occupied molecular orbital (HOMO) with substitution of the equatorial and axial ligands.[7b] For example, the π^*-HOMO in $[Rh_2(O_2CMe)_4(H_2O)_2]$ was altered to σ-HOMO when H_2O was substituted by PPh_3. There are some examples of half-lantern-type complexes with two planar chelate ligands such as bipyridine and phenanthroline.[8] Introduction of two biimidazole ligands to the dirhodium complex is interesting because it would form a new type of hydrogen-bonded dimer. We synthesized half-lantern-type dirhodium complexes with two biimidazole ligands $[Rh_2(O_2CR)_2(H_2bim)_2]^{2+}$ (R = Pr, Bu) and their deprotonated dimerized species $[Rh_2(O_2CR)_2(Hbim)_2]_2$. The latter complexes formed hydrogen-bonded dimers with four complementary NH···N hydrogen bonds. We report here the synthesis, structure, and properties of these complexes and discuss the stability of the mixed-valence state.

Received: December 10, 2014
Published: February 18, 2015

DOI: 10.1021/ic502953b
Inorg. Chem. 2015, 54, 2331−2338

EXPERIMENTAL SECTION

Physical Measurements. ^{1}H NMR spectra were measured on a JEOL ECA600 spectrometer. For some measurements, a sample solution was prepared in a J. Young NMR tube by transferring a dry deuterated solvent using a vacuum line. Electronic absorption spectra were recorded on a Shimadzu UV-3100PC spectrophotometer. IR spectra were obtained using a PerkinElmer Spectrum 400 spectrometer. Elemental analyses were determined with a J-Science Lab Micro Corder JM-10. Cyclic voltammograms (CVs) were measured using a BAS CV-50W electrochemical analyzer employing a conventional three-electrode cell with a glassy-carbon disk working electrode, a platinum wire auxiliary electrode, and a Ag/Ag^+ (0.01 M $AgNO_3$, M = mol dm^{-3}) reference electrode in 0.1 M Bu_4NPF_6 solutions. To correct for the liquid junction potential, the oxidation potential of ferrocene (Fc) was measured in the same electrolytic solution after each CV measurement, and electrode potentials were converted to those relative to Fc/Fc^+.

Materials. Biimidazole was provided by Prof. Tadokoro. $[Rh_2(O_2CBu)_4]$ and $[Rh_2(O_2CPr)_4]$ were prepared by literature methods.[9] Dichloromethane and acetonitrile for CV measurements were distilled from CaH_2 before use. Other reagents were used as received.

Synthesis of $[Rh_2(O_2CBu)_2(H_2bim)_2Cl_2]\cdot H_2O$, $[\mathbf{1}Cl_2]\cdot H_2O$. $[Rh_2(O_2CBu)_4]$ (400 mg, 0.65 mmol) and biimidazole (H_2bim, 180 mg, 1.34 mmol) were placed in a 50 mL flask, and 20 mL of dichloromethane was added. The resulting purple solution was refluxed for 24 h under argon atmosphere. The color of the solution first changed to black, and finally, an olive-green suspension was obtained. The olive-green powder obtained by filtration was dissolved in 0.01 M HCl/MeOH (30 mL). The solution was evaporated to dryness, and the resulting solid was dissolved in methanol and purified using gel filtration with a Sephadex LH-20 column and a methanol eluent. The second cobalt-green band was collected and evaporated to dryness. After washing with diethyl ether and drying under vacuum, 111 mg (0.14 mmol, 21%) of $[\mathbf{1}Cl_2]\cdot H_2O$ was obtained as a cobalt-green solid. Anal. Calcd for $C_{22}H_{32}Cl_2N_8O_5Rh_2$: C, 34.53; H, 4.21; N, 14.64. Found: C, 33.89; H, 4.15; N, 14.50. ^{1}H NMR (600 MHz, CD_3OD): δ 7.12 (s, 4H, biimidazole CH), 6.74 (s, 4H, biimidazole CH), 2.66 (t, 4H, $CH_2CH_2CH_2CH_3$), 1.79 (m, 4H, $CH_2CH_2CH_2CH_3$), 1.48 (m, 4H, $CH_2CH_2CH_2CH_3$), 1.00 (t, 6H, CH_3). UV−vis (MeOH); λ_{max}, nm (ε, M^{-1} cm^{-1}): 266 (32 500), 306 (sh) (12 600), 601 (155).

Synthesis of $[Rh_2(O_2CPr)_2(H_2bim)_2Cl_2]$, $[\mathbf{2}Cl_2]$. $[\mathbf{2}Cl_2]$ was synthesized in a similar manner to $[\mathbf{1}Cl_2]$.Starting with $[Rh_2(O_2CPr)_4]$ (290 mg, 0.52 mmol) and H_2bim (150 mg, 1.12 mmol), $[\mathbf{2}Cl_2]$ (170 mg, 0.24 mmol, 46%) was obtained by recrystallization from methanol. Anal. Calcd for $C_{20}H_{26}Cl_2N_8O_4Rh_2$: C, 33.40; H, 3.64; N, 15.58. Found: C, 33.39; H, 3.91; N, 15.21. ^{1}H NMR (600 MHz, CD_3OD):δ 7.11 (s, 4H, biimidazole CH), 6.75 (s, 4H, biimidazole CH), 2.64 (t, 4H, $CH_2CH_2CH_2CH_3$), 1.84 (m, 4H, $CH_2CH_2CH_2CH_3$), 1.06 (t, 6H, CH_3). UV−vis (MeOH); λ_{max}, nm (ε, M^{-1} cm^{-1}): 267 (33 400), 306 (sh) (12 900), 604 (148).

Synthesis of $[Rh_2(O_2CBu)_2(H_2bim)_2](PF_6)_2$, $[\mathbf{1}](PF_6)_2$. $[Rh_2(O_2CBu)_4]$ (82 mg, 0.13 mmol) and H_2bim (37 mg, 0.27 mmol) were placed in a flask, and 20 mL of dichloromethane was added. Reflux of the solution for 24 h under argon atmosphere afforded an olive-green suspension. The olive-green solid obtained by filtration was dissolved in 25 mL of acetonitrile, and 0.5 mL of HPF_6 was added. The green solid obtained by evaporation was dissolved in MeOH and purified by gel-filtration chromatography with Sephadex LH-20. The green eluate was collected and evaporated to dryness. The resulting green solid was recrystallized from MeCN and dried in vacuo. Yield 38 mg (30%). Anal. Calcd for $C_{22}H_{30}F_{12}N_8O_4P_2Rh_2$: C, 27.35; H, 3.13; N, 11.59. Found: C, 27.81; H, 3.59; N, 11.83. ^{1}H NMR (600 MHz, CD_3CN): δ 13.93 (s, 4H, NH), 6.93 (s, 4H, biimidazole CH), 6.55 (s, 4H, biimidazole CH), 2.54 (t, 4H, $CH_2CH_2CH_2CH_3$), 1.71 (m, 4H, $CH_2CH_2CH_2CH_3$), 1.42 (m, 4H, $CH_2CH_2CH_2CH_3$), 0.98 (t, 6H, CH_3).^{1}H NMR (600 MHz, CD_3OD): δ 7.08 (s, 4H, biimidazole CH), 6.72 (s, 4H, biimidazole CH), 2.64 (t, 4H, $CH_2CH_2CH_2CH_3$), 1.76 (m, 4H, $CH_2CH_2CH_2CH_3$), 1.46 (m, 4H, $CH_2CH_2CH_2CH_3$), 0.98 (t, 6H, CH_3). UV−vis (MeOH); λ_{max}, nm (ε, M^{-1} cm^{-1}): 266 (31 800), 311 (sh) (10 800), 605 (164). UV−vis (MeCN); λ_{max}, nm (ε, M^{-1} cm^{-1}) 265 (29 900), 302 (sh) (15 800), 566 (180).

Synthesis of $[Rh_2(O_2CBu)_2(H_2bim)_2(PPh_3)_2](PF_6)_2$, $[\mathbf{1}(PPh_3)_2](PF_6)_2$. A 50 mg (0.19 mmol) amount of complex $[\mathbf{1}](PF_6)_2$ and 51 mg (0.19 mmol) of triphenylphosphine were dissolved in dichloromethane (5 mL). After the resulting red solution was stirred for 30 min at room temperature, the solvent was evaporated to dryness. The red solid was washed with hexane and dried in vacuo. Yield 50 mg (65%). Anal. Calcd for $C_{58}H_{60}F_{12}N_8O_4P_4Rh_2$: C, 46.73; H, 4.06; N 7.51. Found: C, 46.76; H, 4.19; N, 7.54.^{1}H NMR (600 MHz, CD_2Cl_2): δ 11.29 (s, 4H, NH), 7.36 (t, 6H, Ph), 7.23 (s, 24H, Ph), 6.68 (s, 4H, biimidazole CH), 6.19 (s, 4H, biimidazole CH), 2.51 (t, 4H, $CH_2CH_2CH_2CH_3$), 1.57 (m, 4H, $CH_2CH_2CH_2CH_3$), 1.33 (m, 4H, $CH_2CH_2CH_2CH_3$), 0.89 (t, 6H, CH_3). UV−vis (CH_2Cl_2); λ_{max}, nm (ε, M^{-1} cm^{-1}): 260 (29 800), 276 (sh) (25 200), 318 (sh) (14 000), 410 (34 700), 490 (sh) (5960).

Synthesis of $[Rh_2(O_2CPr)_2(H_2bim)_2(PPh_3)_2]Cl_2\cdot H_2O$, $[\mathbf{2}(PPh_3)_2]Cl_2\cdot H_2O$. $[\mathbf{2}Cl_2]\cdot H_2O$ (24 mg, 0.033 mmol) and triphenylphosphine (17 mg, 0.065 mmol) were stirred in dichloromethane (5 mL) for 30 min at room temperature. The red solution was evaporated to dryness and washed with hexane to afford $[\mathbf{2}(PPh_3)_2]Cl_2\cdot H_2O$. Yield 17 mg (42%). Anal. Calcd for $C_{56}H_{58}Cl_2N_8O_5P_2Rh_2$: C, 53.31; H, 4.63; N, 8.88. Found: C, 53.17; H, 4.57; N, 8.31. ^{1}H NMR (600 MHz, $CDCl_3$): δ 7.36 (t, 6H, Ph), 7.24 (overlapped with $CHCl_3$, Ph), 6.67 (s, 4H, biimidazole CH), 6.10 (s, 4H, biimidazole CH), 2.53 (t, 4H, $CH_2CH_2CH_3$), 1.68 (m, 4H, $CH_2CH_2CH_3$), 1.02 (t, 6H, CH_3).

Synthesis of $[Rh_2(O_2CBu)_2(Hbim)_2(PPh_3)_2]_2$, $[\mathbf{1}'(PPh_3)_2]_2$. $[\mathbf{1}Cl_2]\cdot H_2O$ (50 mg, 0.065 mmol) and triphenylphosphine (46 mg, 0.17 mmol) were stirred in 10 mL of dichloromethane for 30 min. The red solid obtained by evaporation of the solution was dissolved in methanol, and 1.0 mL of 0.01 M KOH aqueous solution was added dropwise. Red needle crystals were filtered and washed with water (30 mg, 39%). Anal. Calcd for $C_{58}H_{58}N_8O_4P_2Rh_2$: C, 58.11; H, 4.88; N, 9.35. Found: C, 57.74; H, 4.90; N, 9.42. ^{1}H NMR (600 MHz, $CDCl_3$): δ 7.27 (s, 6H, Ph), 7.20 (s, 24H, Ph), 6.19 (s, 4H, biimidazole CH), 6.12 (s, 4H, biimidazole CH), 2.47 (t, 4H, $CH_2CH_2CH_2CH_3$), 1.60 (m, 4H, $CH_2CH_2CH_2CH_3$), 1.39 (m, 4H, $CH_2CH_2CH_2CH_3$), 0.92 (t, 6H, CH_3). UV−vis (CH_2Cl_2); λ_{max}, nm (ε, M^{-1} cm^{-1} per one dirhodium unit): 260 (33 900), 285 (sh) (25 300), 355 (34 600),434 (sh) (5500), 668 (336).

Synthesis of $[Rh_2(O_2CPr)_2(Hbim)_2(PPh_3)_2]_2$, $[\mathbf{2}'(PPh_3)_2]_2$. $[\mathbf{2}'(PPh_3)_2]_2$ was synthesized in a similar manner to $[\mathbf{1}'(PPh_3)_2]_2$. Starting with $[\mathbf{2}Cl_2]\cdot H_2O$ (30 mg, 0.041 mmol) and triphenylphosphine (30 mg, 0.11 mmol), red needle crystals of $[\mathbf{2}'(PPh_3)_2]_2$ (15 mg, 32%) were obtained by recrystallization from methanol. Anal. Calcd for $C_{56}H_{54}N_8O_4P_2Rh_2$: C, 57.45; H, 4.65; N, 9.57. Found: C, 57.47; H, 4.76; N, 9.29.

X-ray Structure Determination. Crystals of $[\mathbf{1}Cl_2]\cdot H_2O$ and $[\mathbf{2}Cl_2]\cdot H_2O$ were obtained by slow evaporation of their methanol solutions. Crystals of $[\mathbf{2}(PPh_3)_2]Cl_2\cdot H_2O\cdot C_7H_8$ were grown by slow evaporation of a toluene solution.The diffraction data for $[\mathbf{1}Cl_2]\cdot H_2O$ were obtained on a Rigaku XtaLAB P200 diffractometer using multilayer mirror monochromated Mo Kα (λ = 0.71075 Å) radiation at the Applied Technology Center of Rigaku Co. The X-ray diffraction data for $[\mathbf{2}Cl_2]\cdot H_2O$ and $[\mathbf{2}(PPh_3)_2]Cl_2\cdot H_2O$ were collected on a Rigaku AFC-7R rotating anode diffractometer with a Mercury CCD detector using monochromated Mo Kα radiation (λ = 0.71069 Å). The diffraction data for $[\mathbf{1}'(PPh_3)_2]_2$ were collected on an ADSC Quantum-210 detector with synchrotron radiation (λ = 1.00002 Å) at the 2D SMC beamline of the Pohang Accelerator Laboratory (PAL), South Korea. The diffraction data for $[\mathbf{2}'(PPh_3)_2]_2$ were measured (λ = 0.6883 Å) at the Photon FactoryAdvanced Ring for Pulse X-rays (PF-AR) of the High Energy Accelerator Research Organization (KEK). Data reduction and cell refinement were carried out using CrystalClear. Structure determination was carried out using the free GUI software of Yadokari-XG 2009.[10]All structures were solved by direct methods SIR97[11] and refined by full-matrix least-squares techniques using Shelxl97.[12] The crystal data and structure refinement

DOI: 10.1021/ic502953b
Inorg. Chem. 2015, 54, 2331−2338

Table 1. Crystal Data and Refinement Details

	[**1**Cl_2]·H_2O	[**2**Cl_2]·H_2O	[**2**$(PPh_3)_2$]Cl_2·H_2O·C_7H_8	[**1′**$(PPh_3)_2$]$_2$	[**2′**$(PPh_3)_2$]$_2$
formula	$C_{22}H_{34}Cl_2N_8O_5Rh_2$	$C_{20}H_{30}Cl_2N_8O_5Rh_2$	$C_{63}H_{66}Cl_2N_8O_5P_2Rh_2$	$C_{116}H_{116}N_{16}O_8P_4Rh_4$	$C_{116}H_{116}N_{16}O_8P_4Rh_4$
fw	765.28	737.22	1353.90	2397.76	2341.66
cryst syst	monoclinic	orthorhombic	monoclinic	monoclinic	triclinic
space group	*Cc*	*Fdd*2	*C*2/*c*	*C*2/*c*	*P*-1
a, Å	8.415 (3)	32.518 (10)	44.168 (7)	14.7481 (2)	14.6190 (2)
b, Å	43.040 (12)	41.503 (13)	10.2692 (15)	42.9551 (8)	18.0709 (3)
c, Å	16.659 (5)	8.457 (3)	27.496 (4)	18.1613 (3)	21.7988 (4)
α, deg	90	90	90	90	98.5520 (6)
β, deg	102.833 (7)	90	92.779 (9)	111.3171 (8)	97.2913 (7)
γ, deg	90	90	90	90	110.9130 (11)
V, Å^3	5883 (3)	11414 (6)	12457 (3)	10718.1 (3)	5217.63 (15)
Z	8	16	8	4	2
μ, mm^{-1}	1.35	1.39	0.72	1.72	0.75
T, K	93	293	293	101	90
$R[F^2 > 2\sigma(F^2)]^a$	0.107	0.064	0.111	0.056	0.079
$wR(F^2)^a$	0.278	0.154	0.234	0.159	0.219

$^a R = [(\Sigma||wF_o| - |F_c||)/(\Sigma|F_{o0}|)]^2$; $wR = [(\Sigma w(F_o^2 - F_c^2)^2)/(\Sigma w(F_c^2)^2)]^{1/2}$.

Table 2. Selected Distances (Angstroms) and Angles (deg)

[**1**Cl_2]·H_2O			
Rh1−Rh2	2.541 (2)	Rh3−Rh4	2.530 (2)
Rh1−Cl1	2.532 (5)	Rh3−Cl3	2.538 (5)
Rh2−Cl2	2.590 (5)	Rh4−Cl4	2.609 (5)
Rh2−Rh1−Cl1	170.80 (15)	Rh4−Rh3−Cl3	172.92 (13)
Rh1−Rh2−Cl2	172.28 (13)	Rh3−Rh4−Cl4	172.89 (12)
N1−Rh1−Rh2−N5	−20.2 (7)	N9−Rh3−Rh4−N13	−23.8 (7)
N3−Rh1−Rh2−N7	−19.8 (7)	N11−Rh3−Rh4−N15	−22.5 (7)
O1−Rh1−Rh2−O2	−17.2 (5)	O5−Rh3−Rh4−O6	−19.6 (5)
O3−Rh1−Rh2−O4	−18.4 (5)	O7−Rh3−Rh4−O8	−19.8 (5)
[**2**Cl_2]·H_2O			
Rh1−Rh2	2.5291 (11)	Rh2−Cl2	2.594 (3)
Rh1−Cl1	2.540 (3)		
Rh2−Rh1−Cl1	171.56 (8)	Rh1−Rh2−Cl2	172.38 (6)
N1−Rh1−Rh2−N5	22.3 (3)	O1−Rh1−Rh2−O2	18.8 (3)
N3−Rh1−Rh2−N7	22.4 (3)	O3−Rh1−Rh2−O4	19.1 (3)
[**2**$(PPh_3)_2$]Cl_2·H_2O·C_7H_8			
Rh1−Rh2	2.6112 (9)	Rh2−P2	2.560 (2)
Rh1−P1	2.483 (2)		
Rh2−Rh1−P1	173.48 (7)	Rh1−Rh2−P2	176.07 (7)
N1−Rh1−Rh2−N5	23.8 (3)	O1−Rh1−Rh2−O2	18.5 (3)
N3−Rh1−Rh2−N7	24.6 (3)	O3−Rh1−Rh2−O4	18.6 (3)
[**1′**$(PPh_3)_2$]			
Rh1−Rh1′	2.6329 (14)	Rh2−Rh2′	2.6176 (13)
Rh1−P1	2.509 (3)	Rh2−P2	2.463 (3)
Rh1′−Rh1−P1	175.39 (6)	Rh2′−Rh2−P2	171.09 (8)
N1−Rh1−Rh1′−N3′	−11.1 (4)	N5−Rh2−Rh2′−N7′	−11.5 (4)
O1−Rh1−Rh1′−O2′	−11.8 (3)	O3−Rh2−Rh2′−O4′	−15.6 (2)
[**2′**$(PPh_3)_2$]			
Rh1−Rh2	2.6372 (6)	Rh3−Rh4	2.6202 (6)
Rh1−P1	2.5172 (15)	Rh3−P3	2.4513 (15)
Rh2−P2	2.5395 (15)	Rh4−P4	2.4472 (15)
Rh2−Rh1−P1	175.69 (4)	Rh4−Rh3−P3	171.14 (4)
Rh1−Rh2−P2	173.73(4)	Rh3−Rh4−P4	173.57 (4)
N3−Rh1−Rh2−N7	−12.5 (2)	N11−Rh3−Rh4−N15	−11.6 (2)
N1−Rh1−Rh2−N5	−12.1 (2)	N9−Rh3−Rh4−N13	−11.5 (2)
O1−Rh1−Rh2−O2	−12.63 (17)	O7−Rh3−Rh4−O8	−14.53 (17)
O3−Rh1−Rh2−O4	−12.73 (18)	O5−Rh3−Rh4−O6	−14.45 (16)

results are summarized in Table 1, and selected bond distances and angles are listed in Table 2.

DFT Calculations. Molecular structure calculations were performed using the DFT method with the B3LYP functional as

DOI: 10.1021/ic502953b
Inorg. Chem. 2015, 54, 2331−2338

implemented in the Gaussian09 software package.[13] The LANL2DZ basis set[14] for Rh and the 6-31+G basis sets[15] for the other elements were selected. An effective core potential was used for the rhodium atoms.[14] Models of the neutral complex, $[Rh_2(O_2CMe)_2(Hbim)_2(PMe_3)_2]_2$ ($[\mathbf{3}']_2$), were generated using the geometrical parameters obtained from the crystal structure data of $[\mathbf{1}'(PPh_3)_2]_2$. The geometrical optimization of the one-electron-oxidized form was started from $[Rh_2(O_2CMe)_2(Hbim)_2(PMe_3)_2]_2^+$ ($[\mathbf{3}']_2^+$), $[Rh_2(O_2CMe)_2(H_2bim)(Hbim)(PMe_3)_2][Rh_2(O_2CMe)_2(Hbim)(bim)(PMe_3)_2]^+$ ($[\mathbf{3}' - H][\mathbf{3}' + H]^+$), and $[Rh_2(O_2CMe)_2(H_2bim)_2(PMe_3)_2][Rh_2(O_2CMe)_2(bim)_2(PMe_3)_2]^+$ ($[\mathbf{3}][\mathbf{3}'']^+$) with fixed N−H distances. All optimizations were performed using the polalizable continuum model in a dichloromethane solvent cavity.

RESULTS AND DISCUSSION

Syntheses. The choice of solvent and bridging carboxylates was important for synthesis of the complexes, because complexes with biimidazole ligands often have low solubility in common solvents. Although we tried to synthesize $Rh_2(O_2CR)_2(H_2bim)_2^{2+}$ (R = Me, Et, Ph), mixing solutions of $[Rh_2(O_2CR)_4]$ and biimidazole immediately gave reddish-purple precipitates and the reaction did not proceed. Reaction of $[Rh_2(O_2CR)_4]$ (R = Pr, Bu) with H_2bim in 1,2-dichloroethane gave a reddish-purple solution, and the solution color changed to olive green on heating. The color change indicates that N-coordinated H_2bim moved from the axial to the equatorial sites. The neutral complexes $[\mathbf{1}Cl_2]$ and $[\mathbf{2}Cl_2]$ were easily isolated and characterized by single-crystal X-ray structure determination and ^1H NMR spectra (Figure S1, Supporting Information). The cationic complex was obtained as $[\mathbf{1}]^{2+}$ without axial ligands. It was confirmed by elemental analysis and ^1H NMR spectra. If the complex has one or two axial ligands,which may be acetonitrile or water, one or two equivalents of these molecules would be observed as free molecules in the spectra. However, only a trace amount of free acetonitrile was observed in the CD_3OD solution of $[\mathbf{1}](PF_6)_2$ (Figure S1, Supporting Information). The NH protons were not observed in the spectra of CD_3OD solutions, which is a relatively strong hydrogen bond acceptor, but those for $[\mathbf{1}](PF_6)_2$ were observed in CD_3CN solution. Complexes with axial phosphine ligands were readily synthesized by reaction with PPh_3.

Biimidazolate complexes were synthesized by deprotonation of the corresponding biimidazole complexes using a KOH solution. Although biimidazolate complexes with acetonitrile or pyridine axial ligands are insoluble in common solvents such as acetonitrile, methanol, and dichloromethane, the triphenylphosphine complex is soluble in these solvents. The NMR spectrum of $[\mathbf{1}'(PPh_3)_2]_2$ in CD_2Cl_2 was almost unchanged upon diluting the solution of 3.0 mM to 0.30 mM (Figure S2a,b, Supporting Information). It indicates that the dimer structure is maintained in this concentration range. For both of the solutions, decreasing temperature made a similar slight change of the spectra. This concentration-independent but slightly temperature-dependent change of NMR spectra may be due to a small structural change in the dimer such as shortening of the hydrogen bond distances. The unobserved NH signal for $[\mathbf{1}'(PPh_3)_2]_2$ is consistent with no NH signal in the spectra of CD_3OD solutions of $\mathbf{1}^{2+}$.

Structures. The structure of $[\mathbf{1}Cl_2]$ in $[\mathbf{1}Cl_2]\cdot H_2O$ is shown in Figure 1. In this structure, there are two independent dirhodium complexes in an asymmetric unit. In each complex, two rhodium atoms with biimidazole ligands are bridged by two valerate ions and each rhodium atom is axially coordinated by a

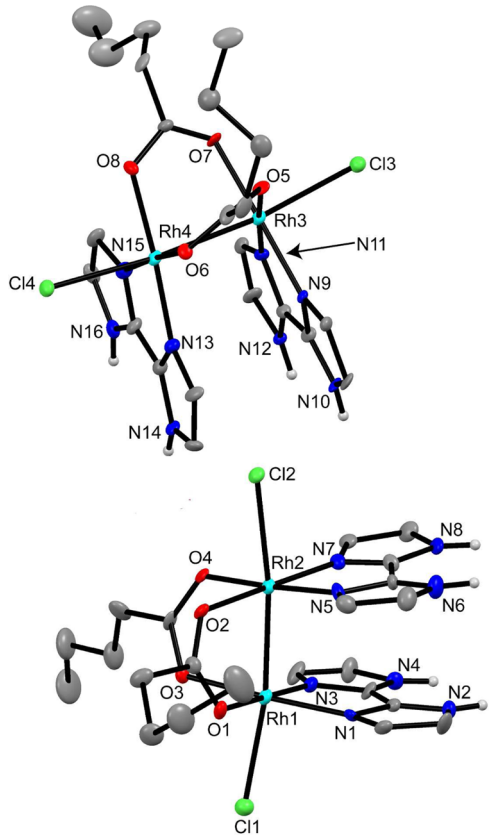

Figure 1. Structure of two independent $[Rh_2(O_2CBu)_2(H_2bim)_2Cl_2]$ ($[\mathbf{1}Cl_2]$) in the crystal of $[\mathbf{1}Cl_2]\cdot H_2O$ showing the atom-labeling scheme. Displacement ellipsoids are drawn at the 30% probability level. H atoms are omitted for clarity except those on N atoms, which are shown as small spheres of arbitrary radii.

chloride ion. The Rh−Rh bond distances of 2.541(2) and 2.530(2) Å are longer than those in paddlewheel complexes $[Rh_2(O_2CMe)_4Cl_2]^{2-}$ (2.387(1)−2.399(1) Å)[16−20] and slightly shorter than that in half-lantern-type dirhodium complexes with planar chelate ligands $[Rh_2(O_2CMe)_2(bpy)_2Cl_2]$ (2.574(1) and 2.601(1) Å),[8c,h] and $[Rh_2(O_2CMe)_2(phen)_2Cl_2]$ (2.554(1) and 2.561(2) Å).[8a] The Rh2−Cl2 (2.590(5) Å) and Rh4−Cl4 (2.609(5) Å) distances are much longer than Rh1−Cl1 (2.532(5) Å) and Rh3−Cl3 (2.538(5) Å), which may be due to a difference of hydrogen-bonding environment where Cl2 and Cl4 accept two hydrogen bonds from a biimidazole ligand and one from a water molecule (O9 and O10) and Cl1 and Cl3 accept one from a biimidazole and one from a water molecule (Figure S3, Supporting Information). Other structural features of this complex are a torsion angle N−Rh−Rh−N of ca. 22° and dihedral angles of the two coordination planes (RhN_2O_2) of ca. 16°.

The structure of $[\mathbf{2}Cl_2]$ and the crystal structure of $[\mathbf{2}Cl_2]\cdot H_2O$ are shown in Figures S4 and S5, Supporting Information, respectively. The structure of $[\mathbf{2}Cl_2]$ is very similar to that of $[\mathbf{1}Cl_2]$ except for a bridging butyrate instead of valerate. The bond distances and angles around the Rh_2 core are very similar to those observed in $[\mathbf{1}Cl_2]$. This means that the alkyl groups of the carboxylate ligands do not affect the core structures of the Rh_2 complexes.

The structure of $[\mathbf{2}(PPh_3)_2]^{2+}$ and the crystal structure of $[\mathbf{2}(PPh_3)_2]Cl_2\cdot H_2O\cdot C_7H_8$ are shown in Figures 2 and S6, Supporting Information, respectively. The Rh−Rh distance of

DOI: 10.1021/ic502953b
Inorg. Chem. 2015, 54, 2331−2338

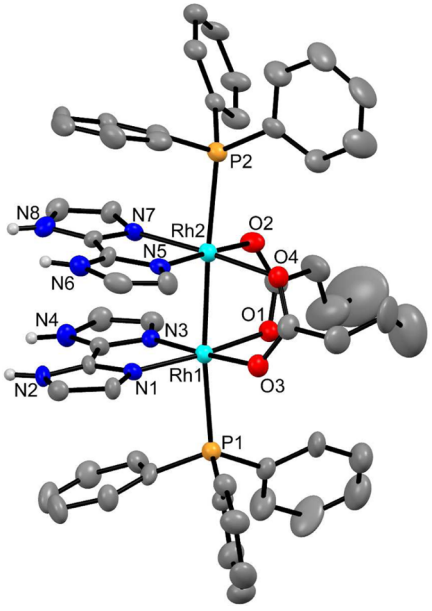

Figure 2. Structure of $[Rh_2(O_2CPr)_2(H_2bim)_2(PPh_3)_2]^{2+}$ ($[\mathbf{2}(PPh_3)_2]^{2+}$) in the crystal of $[\mathbf{2}(PPh_3)_2]Cl_2{\cdot}H_2O{\cdot}C_7H_8$ showing the atom-labeling scheme. Displacement ellipsoids are drawn at the 30% probability level. H atoms are omitted for clarity except those on N atoms, which are shown as small spheres of arbitrary radii.

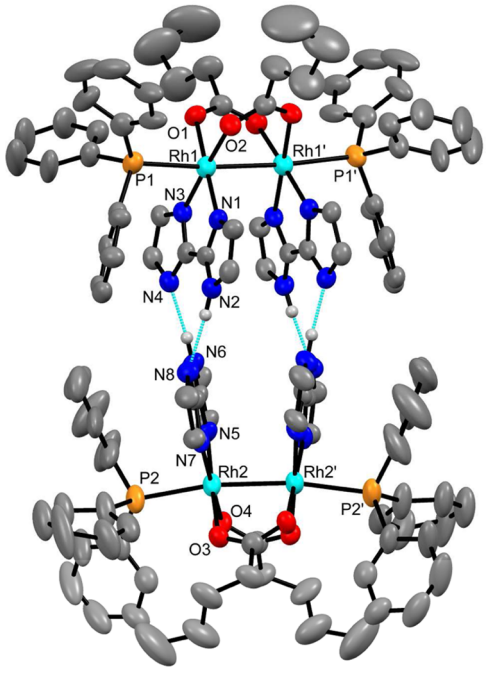

Figure 3. Structure of $[Rh_2(O_2CBu)_2(Hbim)_2(PPh_3)_2]_2$ ($[\mathbf{1}'(PPh_3)_2]_2$) showing the atom-labeling scheme. Displacement ellipsoids are drawn at the 30% probability level. H atoms are omitted for clarity except those on N atoms, which are shown as small spheres of arbitrary radii.

2.6112(9) Å is longer than that in $[\mathbf{1}Cl_2]$ and $[\mathbf{2}Cl_2]$. A longer Rh−Rh distance with axial phosphine ligands ($[Rh_2(O_2CMe)_4(PPh_3)_2]$ 2.451(1) Å)[21]than with chloro ligands[16−20] was also observed in the paddlewheel Rh_2 complex. Other structural features were not changed from $[\mathbf{2}Cl_2]$: the torsion angles of N−Rh−Rh−N are ca. 24°, and the dihedral angle of the two coordination planes (RhN_2O_2) is ca. 15°.

The structure of $[\mathbf{1}'(PPh_3)_2]_2$ shown in Figure 3 is a hydrogen-bonded dimer of the half-lantern complex. The NH of each biimidazolate ($Hbim^-$) ligand donates a hydrogen to the N of $Hbim^-$ on the neighboring complex, and then four hydrogen bonds connect two dirhodium complexes. The dimer lies on a crystallographic 2-fold axis that bisects the two Rh−Rh bonds. The two crystallographically independent dirhodium complexes have similar Rh−Rh bond lengths (2.6329(14), 2.6176(13) Å) to that in $[\mathbf{2}(PPh_3)_2]^{2+}$. The torsion angles of N−Rh−Rh−N are ca. −11°, which is smaller than in $[\mathbf{2}(PPh_3)_2]^{2+}$. The structure of $[\mathbf{2}'(PPh_3)_2]_2$ is very similar to $[\mathbf{1}'(PPh_3)_2]_2$, but there is one independent dimer of dirhodium complexes (Figure S7, Supporting Information). The smaller torsion angle in the biimidazolate complexes may be due to complementary hydrogen bonds between the dirhodium units. Dihedral angles between two $Hbim^-$ ligands on each dirhodium unit are ca. 16°. These angles hindered coplanar self-complementary hydrogen bonds between the biimidazolate ligands on the different dirhodium units. To form hydrogen bonds between the noncoplanar biimidazolate ligands, the Rh2−Rh2′ axis in $[\mathbf{1}'(PPh_3)_2]_2$ was rotated 25.7° from the eclipsed position with the Rh1−Rh1′ around the 2-fold axis and the dihedral angle between the biimidazolate ligands is 34.90(13)° (the corresponding values for $[\mathbf{2}'(PPh_3)_2]_2$ are 28.4° and 36.69(9)° and 35.58(9)°, respectively). The hydrogen-bond distances are 2.752(11) and 2.733(12) Å for $[\mathbf{1}'(PPh_3)_2]_2$ and 2.774(7), 2.737(7), 2.735(6), and 2.732(7) Å for $[\mathbf{2}'(PPh_3)_2]_2$,which are comparable to those in $[ReCl_2(P^nBu_3)_2(Hbim)]_2$. In $[ReCl_2(P^nBu_3)_2(Hbim)]_2$, the NH protons readily exchanged between two biimidazolate ligands because they were able to move along hydrogen bonds and the resulted complex was the same as the original one. On the other hand, if the structure of $[\mathbf{1}'(PPh_3)_2]$ kept on moving the protons from N6 and N2 to N4 and N8, respectively, it makes the resulting NH···N hydrogen bonds less effective (H···N ca. 1.96 Å and N−H···N ca. 147°) than the original ones (H···N ca. 1.88 Å and N−H···N ca. 168°).

Properties. The electronic absorption spectra of $[\mathbf{1}Cl_2]$ in MeOH and $[\mathbf{1}](PF_6)_2$ in MeOH and MeCN are shown in Figure 4. The band at 566 nm for the MeCN solution of

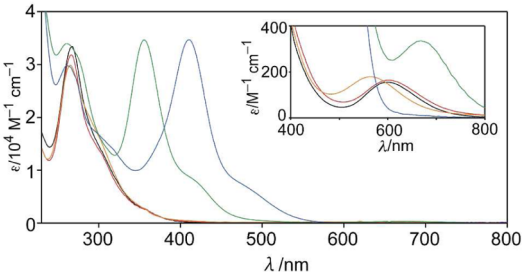

Figure 4. UV−vis absorption spectra of $[\mathbf{1}Cl_2]$ (black) in MeOH, $[\mathbf{1}](PF_6)_2$ in MeOH (red) and in MeCN (orange), and $[\mathbf{1}(PPh_3)_2](PF_6)_2$ (blue) and $[\mathbf{1}'(PPh_3)_2]_2$ (green) in CH_2Cl_2.

$[\mathbf{1}](PF_6)_2$ that can be assigned as a π^*(Rh−Rh) to σ^*(Rh−Rh) transition shifted to 605 nm for the MeOH solution. Similar shifts between N-donor solvents and O-donor solvents have been reported for paddlewheel or other M−M-bonded dirhodium complexes.[8c,22,23] This means that $[\mathbf{1}]^{2+}$ exists as $[\mathbf{1}(MeCN)_2]^{2+}$ and $[\mathbf{1}(MeOH)_2]^{2+}$ in MeCN and MeOH, respectively. The ^1H NMR spectra of $[\mathbf{1}Cl_2]$ and $[\mathbf{1}](PF_6)_2$ in

DOI: 10.1021/ic502953b
Inorg. Chem. 2015, 54, 2331−2338

CD_3OD are quite similar to each other (Figure S1, Supporting Information), but the absorption spectrum for $[\mathbf{1}Cl_2]$ in MeOH is slightly different from that for $[\mathbf{1}](PF_6)_2$ in MeOH. It suggests that the axial chloride ions of $[\mathbf{1}Cl_2]$ do not completely dissociate.

The spectra of $[\mathbf{1}(PPh_3)_2](PF_6)_2$ and $[\mathbf{1}'(PPh_3)_2]_2$ are also shown in Figure 4, from which extinction coefficients of $[\mathbf{1}'(PPh_3)_2]_2$ were calculated per dirhodium complex. $[\mathbf{1}(PPh_3)_2](PF_6)_2$ shows a relatively intense band at 408 nm. Phosphine-coordinated paddlewheel complexes $[Rh_2(O_2CR)_4(PR_3)_2]$ (R = Ph, cyclohexyl) showed an absorption band in this region, and it was assigned to a σ(Rh−Rh) to σ^*(Rh−Rh) transition.[24] The most intense band of $[\mathbf{1}'(PPh_3)_2]_2$ was observed in a higher energy region than that of $[\mathbf{1}(PPh_3)_2](PF_6)_2$.

The CV of $[\mathbf{1}](PF_6)_2$ in CH_3CN (Figure S8, Supporting Information) did not show any clear redox process between −2.1 and 1.9 V. However, $[\mathbf{1}(PPh_3)_2](PF_6)_2$ and $[\mathbf{1}'(PPh_3)_2]_2$ in CH_2Cl_2 showed some oxidation processes, as shown in Figure 5. The biimidazole complex monomer $[\mathbf{1}(PPh_3)_2](PF_6)_2$

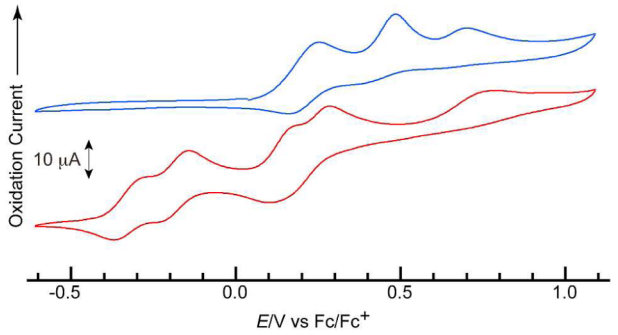

Figure 5. CVs of $[\mathbf{1}(PPh_3)_2](PF_6)_2$ (blue) and $[\mathbf{1}'(PPh_3)_2]$ (red) in 0.1 M Bu_4NPF_6/CH_2Cl_2 using a glassy-carbon disk working electrode, a platinum wire auxiliary electrode, and a Ag/Ag^+ reference electrode. Electrode potentials were converted to those relative to Fc/Fc^+.

exhibits one quasireversible ($E_{1/2}$ = 0.208 V) and two irreversible oxidation waves (E_{pa} = 0.484 and 0.697 V). The first quasireversible oxidation wave can be assigned to oxidation of the dirhodium core Rh_2^{4+}/Rh_2^{5+} and the second one to Rh_2^{5+}/Rh_2^{6+}. On the other hand, the biimidazolate complex dimer $[\mathbf{1}'(PPh_3)_2]_2$ shows two sets of two successive quasireversible oxidation waves and one irreversible oxidation wave. The first successive quasireversible processes at $E_{1/2}$ = −0.325 and−0.186 V can be assigned to $Rh_2^{4+}Rh_2^{4+}/Rh_2^{4+}Rh_2^{5+}$ and $Rh_2^{4+}Rh_2^{5+}/Rh_2^{5+}Rh_2^{5+}$, respectively, and the potential of the first oxidation process for the neutral complex $[\mathbf{1}'(PPh_3)_2]_2$ was ca. 0.5 V shifted toward negative potential compared with the divalent cation $[\mathbf{1}(PPh_3)_3]^{2+}$.

To confirm the assignment of these oxidation processes and determine the electronic state of the oxidized species, ESR spectra of the electrochemically oxidized species were measured. Although bulk electrolysis of $[\mathbf{1}(PPh_3)_2](PF_6)_2$ at 0.23 V in a 0.1 M Bu_4NPF_6/CH_2Cl_2 solution showed a change of the solution color from red to green, the green color readily degraded and finally a yellow solution was obtained. The frozen yellow solution did not show any ESR signals at 77 K. We tried to prepare the sample for ESR by quickly freezing the electrolyzed green solution, but the solution color changed to yellow during the transfer of the solution to an ESR tube, and ESR signals were not obtained. This instability of the oxidized species may be due to the σ(Rh−Rh) HOMO of $[\mathbf{1}(PPh_3)_3]^{2+}$ from which the removal of one electron decrease the bond order of Rh−Rh to 0.5.

During bulk electrolysis of $[\mathbf{1}'(PPh_3)_2]_2$ at −0.29 V, the solution color changed from red to bluish green. When about one-half of the dirhodium complexes were one-electron oxidized based on coulometry, the ESR spectrum of the solution was measured at 77 K. The spectrum shown in Figure 6 is axially symmetrical with hyperfine structure. The g values of

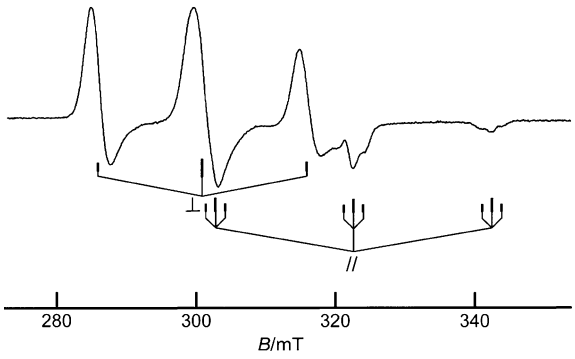

Figure 6. ESR spectrum of electrochemically oxidized $[\mathbf{1}'(PPh_3)_2]_2^+$ in frozen CH_2Cl_2 solution including 0.1 M n-Bu_4NPF_6 at 77 K.

$g_\perp$ = 2.14 and $g_\parallel$ = 2.00 and the hyperfine coupling constants of $A_\perp$(P) = 14.9 mT, $A_\parallel$(P) = 19.8 mT, and $A_\parallel$(Rh) = 1.54 mT resemble those observed for $[Rh_2(O_2CR)_4(PPh_3)_2]^+$.[25] The g values and the hyperfine constants mean that the singly occupied molecular orbital (SOMO) is a Rh−Rh σ orbital that also has a Rh−P σ^* character and the odd electron is localized on one of the two dirhodium units. Therefore, the assignment of the first two consecutive oxidation processes is confirmed as stepwise oxidation of the two dirhodium units. Although the one-electron-oxidized species is stable during the CV measurement, it decomposed slowly and the two-electron-oxidized species cannot be isolated.

Successive oxidation of two dirhodium units in $[\mathbf{1}'(PPh_3)_2]_2$ indicates the existence of a relatively stable mixed-valence state. In the electronic spectra of the electrochemically generated $[\mathbf{1}'(PPh_3)_2]_2^+$, there was no IVCT band in the near IR region (Figure S9, Supporting Information). Considering the orbital symmetry, the σ(Rh−Rh) HOMOs of the two dirhodium units do not interact with each other via the biimidazolate ligands because the σ orbital cannot interact with π-type orbitals on planar equatorial ligands. This is consistent with the localized SOMO on one dirhodium unit from ESR spectra. The thermodynamic stability of the mixed-valence compound with respect to the neutral and doubly oxidized forms was evaluated with the equilibrium constant $K_c = [\mathbf{1}'_2{}^+]^2/[\mathbf{1}'_2][\mathbf{1}'_2{}^{2+}]$, which is calculated as $K_c = \exp(\Delta E_{1/2}/25.69\ \text{mV})$. K_c values for the oxidized and reduced species of $[Re^{III}Cl_2(PBu_3)_2(Hbim)]_2$ are 5.41×10^4 and 1.14×10^4, respectively, as calculated from the redox potentials.[4] The values for the dimers of dimolybdenum complexes are 111−487.[5,6] $[\mathbf{1}'(PPh_3)_2]_2^+$ has a similar value, K_c = 224, to the dimolybdenum species and this means that $[\mathbf{1}'(PPh_3)_2]_2^+$ has comparable stability to the doubly H-bonded dimer of dimolybdenum complexes; nevertheless, H bonds between the complexes are not coplanar.

Theoretical Calculations. The mixed-valence complex for the oxidation of $[\mathbf{1}'(PPh_3)_2]_2$ could not be isolated because it readily decomposed. We discuss the stability of the mixed-

DOI: 10.1021/ic502953b
Inorg. Chem. 2015, 54, 2331−2338

valence state in the oxidation of $[\mathbf{1}'(PPh_3)_2]_2$ with DFT calculations of a model compound $[Rh_2(O_2CMe)_2(Hbim)_2(PMe_3)_2]_2$ ($[\mathbf{3}']_2$). The structure was optimized in C_2 symmetry, and calculated lengths are summarized in Table 3.

Table 3. Averaged Bond Lengths (Angstroms) for X-ray Structures of $[\mathbf{1}'(PPh_3)_2]_2$ and $[\mathbf{2}'(PPh_3)_2]_2$ and the Optimized Geometry of $[\mathbf{3}']_2$ and $[\mathbf{3}][\mathbf{3}'']^+$

	$[\mathbf{1}'(PPh_3)_2]$	$[\mathbf{2}'(PPh_3)_2]$	$[\mathbf{3}']_2$	$[\mathbf{3}][\mathbf{3}'']^+$
Rh−Rh	2.625	2.628	2.680	2.685,[a] 2.883[b]
Rh−O	2.066	2.063	2.117	2.102,[a] 2.117[b]
Rh−N	2.014	2.020	2.057	2.061,[a] 2.035[b]
Rh−P	2.486	2.488	2.547	2.532,[a] 2.357[b]

[a]Distances for $[\mathbf{3}]^{2+}$. [b]Distances for $[\mathbf{3}'']^-$.

Although the calculated distances around the rhodium atoms are slightly longer than those observed in $[\mathbf{1}'(PPh_3)_2]_2$ and $[\mathbf{2}'(PPh_3)_2]_2$, the dimer structure was well reproduced. The HOMOs of $[\mathbf{3}']_2$ are σ(Rh−Rh) orbitals on two dirhodium cores, which is consistent with the experimental results (Figure S10, Supporting Information).

Geometry optimization of the cation was started from three types of hydrogen-bonded dimers, $[\mathbf{3}']_2^+$, $[Rh_2(O_2CMe)_2(H_2bim)(Hbim)(PMe_3)_2][Rh_2(O_2CMe)_2(Hbim)(bim)(PMe_3)_2]^+$ ($[\mathbf{3}' + H][\mathbf{3}' - H]^+$), and $[Rh_2(O_2CMe)_2(H_2bim)_2(PMe_3)_2][Rh_2(O_2CMe)_2(bim)_2(PMe_3)_2]^+$($[\mathbf{3}][\mathbf{3}'']^+$) with fixed NH distances. The optimized structures for $[\mathbf{3}']_2^+$ and $[\mathbf{3}' + H][\mathbf{3}' - H]^+$were not obtained, and only $[\mathbf{3}][\mathbf{3}'']^+$ gave the structure as a one-electron-oxidized $[\mathbf{3}'']^-$ hydrogen bonded with a biimidazole complex $[\mathbf{3}]^{2+}$. The Rh−Rh distance of the one-electron-oxidized unit $[\mathbf{3}'']^-$ is much longer than that in $[\mathbf{3}]^{2+}$ because the SOMO is σ(Rh−Rh) of $[\mathbf{3}'']^-$ (Figure S11, Supporting Information). This is consistent with the ESR spectra, which indicate localization of the odd electron on one dirhodium unit. Transfer of two NH hydrogens from one dirhodium complex to the other produces another structural change. The rotation angles of Rh−Rh bonds around the axis through the centers of the Rh−Rh bonds are 18.58° in $[\mathbf{3}']_2$. The angle in $[\mathbf{3}][\mathbf{3}'']^+$ of 15.64° is narrower than that. If the proton transfer occurs in the geometry of $[\mathbf{3}']_2$, hydrogen bonds from the transferred proton are bent (the angle of N−H···N is about 153°). However, elongation of the Rh−Rh bond in $[\mathbf{3}'']^-$ and the smaller rotation angle in $[\mathbf{3}][\mathbf{3}'']^+$ made the N−H···N angle closer to linear. These structural changes stabilize the mixed-valence state.

CONCLUSIONS

Quadruply hydrogen-bonded dimer complexes with biimidazolate, $[\mathbf{1}'(PPh_3)_2]_2$ and $[\mathbf{2}'(PPh_3)_2]_2$, have been synthesized and characterized. $[\mathbf{2}'(PPh_3)_2]_2$ shows a relatively stable mixed-valence state in spite of noncoplanar complementary hydrogen bonds between the biimidazolate ligands. A theoretical calculation shows that the proton-coupled mixed-valence complex of $[\mathbf{3}][\mathbf{3}'']^+$ may be stabilized with the motion of dirhodium complexes along with the transfer of an electron and protons. Unfortunately, isolation of the oxidized species was not successful because it is stable only on a CV time scale. This may be due to σ(Rh−Rh) HOMOs in $[\mathbf{1}'(PPh_3)_2]_2$ from which removal of an electron weakens the Rh−Rh bond. The better stability for $[\mathbf{1}'(PPh_3)_2]_2^+$ than for $[\mathbf{1}(PPh_3)_2]^{3+}$ may be due to restriction in breaking the Rh−Rh bonds in $[\mathbf{1}''(PPh_3)_2]_2^+$ by hydrogen bonds between the units and/or decreased repulsion of the rhodium atoms in the deprotonated anionic complex. The HOMO of the dirhodium complexes could be changed with bridging and axial ligands: for example, π-donor bridging ligands raise the δ*(Rh−Rh) orbital. Isolation and structure determination of this type of mixed-valence compound with another HOMO is our next target.

ASSOCIATED CONTENT

Supporting Information

Crystallographic data in CIF format; ^{1}H NMR spectra of $[\mathbf{1}Cl_2]\cdot H_2O$, $[\mathbf{1}](PF_6)_2$, $[\mathbf{1}(PPh_3)_2](PF_6)_2$, $[\mathbf{1}'(PPh_3)_2]_2$, $[\mathbf{2}Cl_2]\cdot H_2O$, and $[\mathbf{2}(PPh_3)_2]Cl_2\cdot H_2O$; X-ray structures of $[\mathbf{1}Cl_2]\cdot H_2O$, $[\mathbf{2}Cl_2]\cdot H_2O$, $[\mathbf{2}(PPh_3)_2]Cl_2\cdot H_2O$, and $[\mathbf{2}'(PPh_3)_2]_2$; CVs of $[\mathbf{1}](PF_6)_2$ in MeCN; UV−vis spectra of electrochemically oxidized species of $[\mathbf{1}'(PPh_3)_2]_2$; DFT calculations of $[\mathbf{3}']_2$ and $[\mathbf{3}]^{2+}[\mathbf{3}'']^-$. This material is available free of charge via the Internet at http://pubs.acs.org.

AUTHOR INFORMATION

Corresponding Author

*E-mail: ebihara@gifu-u.a.jp.

Notes

The authors declare no competing financial interest. The authors declare no competing financial interest.

ACKNOWLEDGMENTS

Computations were performed at the Research Center for Computational Science, Okazaki, Japan. We thank Professor H. Wasada and Professor T. Hashimoto (Gifu University) for helpful advice and support concerning the theoretical calculations. Part of this work has been performed under the approval of the Photon Factory Program Advisory Committee (Proposal No. 2014P004). We thank Professor M. Kawano and Dr. T. Kojima (POSTECH) for assistance in the collection of X-ray diffraction data with the synchrotron radiation source. We thank Rigaku Corp. for X-ray data collection. We also thank Professor M. Tadokoro (Tokyo University of Science) for provision of biimidazole and helpful discussion. This work was supported by JSPS KAKENHI Grant Nos. 22550058 and 26410068.

REFERENCES

(1) Sun, H.; Steeb, J.; Kaifer, A. E. *J. Am. Chem. Soc.* **2006**, *128*, 2820−2821.

(2) Goeltz, J. C.; Kubiak, C. P. *J. Am. Chem. Soc.* **2010**, *132*, 17390−17392.

(3) Canzi, G.; Goeltz, J. C.; Henderson, J. S.; Park, R. E.; Maruggi, C.; Kubiak, C. P. *J. Am. Chem. Soc.* **2014**, *136*, 1710−1713.

(4) Tadokoro, M.; Inoue, T.; Tamaki, S.; Fujii, K.; Isogai, K.; Nakazawa, H.; Takeda, S.; Isobe, K.; Koga, N.; Ichimura, A.; Nakasuji, K. *Angew. Chem., Int. Ed.* **2007**, *46*, 5938−5942.

(5) Wilkinson, L. A.; McNeill, L.; Meijer, A. J. H. M.; Patmore, N. J. *J. Am. Chem. Soc.* **2013**, *135*, 1723−1726.

(6) Wilkinson, L. A.; McNeill, L.; Scattergood, P. A.; Patmore, N. J. *Inorg. Chem.* **2013**, *52*, 9683−9691.

(7) (a) Kawamura, T.; Ebihara, M.; Miyamoto, M. *Chem. Lett.* **1993**, 1509−1512. (b) Kawamura, T.; Maeda, M.; Miyamoto, M.; Usami, H.; Imaeda, K.; Ebihara, M. *J. Am. Chem. Soc.* **1998**, *120*, 8136−8142. (c) Kawamura, T.; Kachi, H.; Fujii, H.; Kachi-Terajima, C.; Kawamura, Y.; Kanematsu, N.; Ebihara, M.; Sugimoto, K.; Kuroda-Sowa, T.; Munakata, M. *Bull. Chem. Soc. Jpn.* **2000**, *73*, 657−668. (d) Yang, Z.; Fujinami, T.; Ebihara, M.; Nakajima, K.; Kitagawa, H.; Kawamura, T. *Chem. Lett.* **2000**, 1006−1007. (e) Yang, Z.; Ebihara, M.; Kawamura, T.; Okubo, T.; Mitani, T. *Inorg. Chim. Acta* **2001**, *321*, 97−106.

DOI: 10.1021/ic502953b
Inorg. Chem. 2015, 54, 2331−2338

(f) Takazaki, Y.; Yang, Z.; Ebihara, M.; Inoue, K.; Kawamura, T. *Chem. Lett.* **2003**, *32*, 120−121. (g) Fuma, Y.; Ebihara, M.; Kutsumizu, S.; Kawamura, T. *J. Am. Chem. Soc.* **2004**, *126*, 12238−12239. (h) Ebihara, M.; Fuma, Y. *Acta Crystallogr.* **2006**, *C62*, m556−558. (i) Fuma, Y.; Ebihara, M. *Chem. Lett.* **2006**, *35*, 1298−1299. (i) Yang, Z.; Ebihara, M.; Kawamura, T. *Inorg. Chim. Acta* **2006**, *359*, 2465−2471. (j) Fuma, Y.; Miyashita, O.; Kawamura, T.; Ebihara, M. *Dalton Trans.* **2012**, *41*, 8242−8251. (k) Ebihara, M.; Fuma, Y. *Acta Crystallogr.* **2013**, *B69*, 480−489. (l) Uemura, K.; Fukui, K.; Yamasaki, K.; Matsumoto, K.; Ebihara, M. *Inorg. Chem.* **2010**, *49*, 7323−7330. (m) Uemura, K.; Ebihara, M. *Inorg. Chem.* **2011**, *50*, 7919−7921. (n) Uemura, K.; Ebihara, M. *Inorg. Chem.* **2013**, *52*, 5535−5550. (o) Uemura, K.; Kanbara, T.; Ebihara, M. *Inorg. Chem.* **2014**, *53*, 4621−4628.

(8) (a) Glowiak, T.; Pruchnik, F. P.; Zuber, M. *Polym. J. Chem.* **1991**, *65*, 1749−1754. (b) Crawford, C. A.; Matonic, J. H.; Huffman, J. C.; Folting, K.; Dunbar, K. R.; Christou, G. *Inorg. Chem.* **1997**, *36*, 2361−2371. (c) Galdecka, E.; Galdecki, Z.; Pruchnik, F. P.; Jakimowicz, P. *Transition Met. Chem.* **2000**, *25*, 315−319. (d) Pruchnik, F. P.; Jakimowicz, P.; Ciunik, Z.; Stanislawek, K.; Oro, L. A.; Tejel, C.; Ciriano, M. A. *Inorg. Chem. Commun.* **2001**, *4*, 19−22. (e) Chifotides, H. T.; Catalan, K. V.; Dunbar, K. R. *Inorg. Chem.* **2003**, *42*, 8739−8747. (f) Pruchnik, F. P.; Jutarska, A.; Ciunik, Z.; Pruchnik, M. *Inorg. Chim. Acta* **2003**, *350*, 609−616. (g) Yoshimura, T.; Umakoshi, K.; Sasaki, Y. *Inorg. Chem.* **2003**, *42*, 7106−7115. (h) Pruchnik, F. P.; Jutarska, A.; Ciunik, Z.; Pruchnik, M. *Inorg. Chim. Acta* **2004**, *357*, 3019−3026. (i) Cwikowska, M.; Pruchnik, F. P.; Pavlyuk, O.; Lafolet, F.; Chardon-Noblat, S.; Deronzier, A. *Polyhedron* **2010**, *29*, 3059−3065.

(9) Pruchnik, F. P.; Bien, M.; Lachowicz, T. *Met.-Based Drugs* **1996**, *3*, 185−195.

(10) Wakita, K. *Yadokari-XG, Software for Crystal Structure Analyses*; 2001. Kabuto, C.; Akine, S.; Nemoto, T.; Kwon, E. *J. Cryst. Soc. Jpn.* **2009**, *51*, 218.

(11) Altomare, A.; Burla, M. C.; Camalli, M.; Cascarano, G. L.; Giacovazzo, C.; Guagliardi, A.; Moliterni, A. G. G.; Polidori, G.; Spagna, R. *J. Appl. Crystallogr.* **1999**, *32*, 115−119.

(12) Sheldrick, G. M. *Acta Crystallogr.* **2008**, *A64*, 112−122.

(13) Frisch, M. J.; Trucks, G. W.; Schlegel, H. B.; Scuseria, G. E.; Robb, M. A.; Cheeseman, J. R.; Scalmani, G.; Barone, V.; Mennucci, B.; Petersson, G. A.; Nakatsuji, H.; Caricato, M.; Li, X.; Hratchian, H. P.; Izmaylov, A. F.; Bloino, J.; Zheng, G.; Sonnenberg, J. L.; Hada, M.; Ehara, M.; Toyota, K.; Fukuda, R.; Hasegawa, J.; Ishida, M.; Nakajima, T.; Honda, Y.; Kitao, O.; Nakai, H.; Vreven, T.; J. A. Montgomery, J.; Peralta, J. E.; Ogliaro, F.; Bearpark, M.; Heyd, J. J.; Brothers, E.; Kudin, K. N.; Staroverov, V. N.; Kobayashi, R.; Normand, J.; Raghavachari, K.; Rendell, A.; Burant, J. C.; Iyengar, S. S.; Tomasi, J.; Cossi, M.; Rega, N.; Millam, J. M.; Klene, M.; Knox, J. E.; Cross, J. B.; Bakken, V.; Adamo, C.; Jaramillo, J.; Gomperts, R.; Stratmann, R. E.; Yazyev, O.; Austin, A. J.; Cammi, R.; Pomelli, C.; Ochterski, J. W.; Martin, R. L.; Morokuma, K.; Zakrzewski, V. G.; Voth, G. A.; Salvador, P.; Dannenberg, J. J.; Dapprich, S.; Daniels, A. D.; Farkas, Ö.; Foresman, J. B.; Ortiz, J. V.; Cioslowski, J.; Fox, D. J. *Gaussian 09*, Revision D.01; Gaussian, Inc.: Wallingford, CT, 2009.

(14) Hey, P. J.; Watt, W. R. *J. Chem. Phys.* **1985**, *82*, 870−874.

(15) Ditchfield, R.; Hehre, W. J.; Pople, J. A. *J. Chem. Phys.* **1971**, *54*, 724−728.

(16) Dikareva, L. M.; Sadikov, G. G.; Baranovskii, I. B.; Porai-Koshits, M. A. *Russ. J. Inorg. Chem.* **1980**, *25*, 1725−1726.

(17) Miskowski, V. M.; Schaefer, W. P.; Sadeghi, B. S.; Santarsiero, B. D.; Gray, H. B. *Inorg. Chem.* **1984**, *23*, 1154−1162.

(18) Miskowski, V. M.; Dallinger, R. F.; Christoph, G. G.; Morris, D. E.; Spies, G. H.; Woodruff, W. H. *Inorg. Chem.* **1987**, *26*, 2127−2132.

(19) Galdecka, E.; Galdecki, Z.; Pruchnik, F. P.; Starosta, R. *Transition Met. Chem.* **1999**, *24*, 100−103.

(20) Varshavskii, Y. S.; Cherkasova, T. G.; Bikol'skii, A. B.; Vorontsov, I. I. *Russ. J. Inorg. Chem.* **2001**, *46*, 685.

(21) Christoph, G. G.; Halpern, J.; Khare, G. P.; Koh, Y. B.; Romanowski, C. *Inorg. Chem.* **1981**, *20*, 3029−3037.

(22) Yaman, S. O.; Onal, A. M.; Isci, H. *Z. Naturforsch., B* **2003**, *58*, 563−570.

(23) Rak, M.; Pruchnik, F. P.; Ciunik, L. Z.; Lafolet, F.; Chardon-Noblat, S.; Deronzier, A. *Eur. J. Inorg. Chem.* **2009**, 111−118.

(24) Sowa, T.; Kawamura, T.; Shida, T.; Yonezawa, T. *Inorg. Chem.* **1983**, *22*, 56−57.

(25) (a) Kawamura, T.; Fukamachi, K.; Hayashida, S. *J. Chem. Soc., Chem. Commun.* **1979**, 945−946. (b) Kawamura, T.; Fukamachi, K.; Sowa, T.; Hayashida, S.; Yonezawa, T. *J. Am. Chem. Soc.* **1981**, *103*, 364−369.

DOI: 10.1021/ic502953b
Inorg. Chem. 2015, 54, 2331−2338